

PAPER • OPEN ACCESS

X-ray CT adaptation based on a 2D–3D deformable image registration framework using simulated in-room proton radiographies

To cite this article: Prasannakumar Palaniappan *et al* 2022 *Phys. Med. Biol.* **67** 045003

View the [article online](#) for updates and enhancements.

You may also like

- [Experimental comparison of clinically used ion beams for imaging applications using a range telescope](#)
Benedikt Kopp, Sebastian Meyer, Chiara Gianoli *et al.*
- [Proton radiography and proton computed tomography based on time-resolved dose measurements](#)
Mauro Testa, Joost M Verburg, Mark Rose *et al.*
- [Patient-specific CT calibration based on ion radiography for different detector configurations in \$^1\text{H}\$, \$^4\text{He}\$ and \$^{12}\text{C}\$ ion pencil beam scanning](#)
Chiara Gianoli, Maximilian Göppel, Sebastian Meyer *et al.*

VERIQA
RT MonteCarlo 3D
Plan selected. Plan verified.
In less than 3 minutes.

Automated. Independent. Web-Based.

PTW THE DOSIMETRY COMPANY

Explore the benefits of streamlined patient QA



PAPER

X-ray CT adaptation based on a 2D–3D deformable image registration framework using simulated in-room proton radiographies



OPEN ACCESS

RECEIVED
16 July 2021REVISED
18 January 2022ACCEPTED FOR PUBLICATION
25 January 2022PUBLISHED
9 February 2022

Original content from this work may be used under the terms of the [Creative Commons Attribution 4.0 licence](#).

Any further distribution of this work must maintain attribution to the author(s) and the title of the work, journal citation and DOI.



Prasannakumar Palaniappan¹, Sebastian Meyer^{1,3} , Martin Rädler¹, Florian Kamp^{2,4}, Claus Belka², Marco Riboldi¹, Katia Parodi¹  and Chiara Gianoli¹

¹ Department of Medical Physics—Experimental Physics, Ludwig-Maximilians-Universität München, Munich, Germany

² Department of Radiation Oncology, Universitätsklinikum der Ludwig-Maximilians-Universität München, Munich, Germany

³ Now at: Department of Medical Physics, Memorial Sloan Kettering Cancer Center, New York, NY, United States of America.

⁴ Now at: Klinik und Poliklinik für Radioonkologie, Cyberknife und Strahlentherapie, Uniklinik Köln, Köln, Germany.

E-mail: P.Palaniappan@physik.uni-muenchen.de

Keywords: proton radiographies, deformable image registration, adaptive radiation therapy

Abstract

The aim of this work is to investigate in-room proton radiographies to compensate realistic rigid and non-rigid transformations in clinical-like scenarios based on 2D–3D deformable image registration (DIR) framework towards future clinical implementation of adaptive radiation therapy (ART). Monte Carlo simulations of proton radiographies (pRads) based on clinical x-ray CT of a head and neck, and a brain tumor patients are simulated for two different detector configurations (i.e. integration-mode and list-mode detectors) including high and low proton statistics. A realistic deformation, derived from cone beam CT of the patient, is applied to the treatment planning CT. Rigid inaccuracies in patient positioning are also applied and the effect of small, medium and large fields of view (FOVs) is investigated. A stopping criterion, as desirable in realistic scenarios devoid of ground truth proton CT (pCT), is proposed and investigated. Results show that rigid and non-rigid transformations can be compensated based on a limited number of low dose pRads. The root mean square error with respect to the pCT shows that the 2D–3D DIR of the treatment planning CT based on 10 pRads from integration-mode data and 2 pRads from list-mode data is capable of achieving comparable accuracy ($\sim 90\%$ and $>90\%$, respectively) to conventional 3D–3D DIR. The dice similarity coefficient over the segmented regions of interest also verifies the improvement in accuracy prior to and after 2D–3D DIR. No relevant changes in accuracy are found between high and low proton statistics except for 2 pRads from integration-mode data. The impact of FOV size is negligible. The convergence of the metric adopted for the stopping criterion indicates the optimal convergence of the 2D–3D DIR. This work represents a further step towards the potential implementation of ART in proton therapy. Further computational optimization is however required to enable extensive clinical validation.

Introduction

Proton computed tomography (pCT) is intensively investigated as a potential replacement for treatment planning in proton therapy (Parodi 2014, Johnson 2017, Meyer *et al* 2019, Meyer *et al* 2021). The rationale relies on the potential replacement of the empirically calibrated x-ray treatment planning CT with more accurate tissue relative (to water) stopping power (RSP). The pCT is obtained by means of tomographic image reconstruction of proton radiographies (pRads), as the water equivalent thickness (WET) measured by the pRad can be modeled as the integral RSP along the proton trajectory. For this reason, the most promising detectors for pCT have been conceived as combination and synchronization of trackers with an absorption detector to measure the WET for each individual proton, so called in ‘list-mode’ (Schneider *et al* 2005, Schulte *et al* 2008). Tracking systems typically consist of thin silicon strips upstream and downstream the object of interest.

Individual ions are therefore tracked and fully absorbed. The absorption detector can be designed either as a range telescope made of a series of absorption layers interleaved by detection layers or as a single or segmented calorimeter measuring the energy loss and thus, the range of the energetic ions traversing the object of interest. The residual energy or range is calibrated to WET relying on proper detector calibration. List-mode data are defined by assigning the WET to the tracked ion (Sølie *et al* 2020). Simplified imaging prototypes composed by only the absorption detector without tracking system have been proposed for pencil beams, typically referred to as ‘integration-mode’ detectors. This detector configuration infers the mixed residual energy or range components of the pencil beam (due to lateral inhomogeneity) through either the total energy loss in multiple absorption and detection layers or the time resolved energy loss of multiple initial beam energies in a single thin absorption and detection layer. These mixed components for each pencil beam can be resolved by means of linear decomposition of the spatial signal (total energy loss in multiple absorption and detection layers) or the temporal signal (energy loss in a single thin absorption and detection layer). This way, information about range variations due to lateral inhomogeneities can be retrieved. Relying on the calibration of the resolved components to WET, a WET histogram expressing the relative occurrence of each WET component is obtained for each pencil beam (Schneider and Pedroni 1995, Meyer *et al* 2017). Integration-mode data are defined by the WET histogram assigned to the straight pencil beam direction, as provided by the synchronization of the absorption detector with the pencil beam scanning system. The WET histogram enables the computation of a weighted mean WET (WET components weighted by the relative occurrences and averaged) and a mode WET (WET component with the most frequent relative occurrence), thus referring to integration-mode mean and mode, respectively.

The role of the Rads standalone has been pioneered in the context of treatment (range) verification already in the 1990s (Schneider and Pedroni 1995). The measured WET can be compared to the expected one derived from the calibrated x-ray CT and in case of relevant mismatches, the subsequent (or remaining) fraction of the treatment delivery can be paused and the treatment planning CT can be repeated for re-planning. When patient positioning verification is performed relying on in-room tomographic imaging prior to treatment delivery, treatment adaptation is enabled, according to the commonly defined adaptive radiation therapy (ART). Typically, x-ray cone beam computed tomography (CBCT) is mounted on rotating beam gantry, nozzle, robotic arm and even the treatment couch, perpendicular to the therapeutic beam direction (Fattori *et al* 2015, Landry and Hua 2018). The deformation field expressing the inter-fractional anatomical changes between the CBCT and the treatment planning CT is derived by means of deformable image registration (DIR) (Peroni *et al* 2012, Landry *et al* 2015, Park *et al* 2015) based on tomographic (‘3D’) imaging, thus 3D–3D DIR. The deformed treatment planning CT is then adopted to repeat the treatment planning. Alternatively, when scatter correction is applied, the treatment planning is recalculated directly based on the CBCT (Kurz *et al* 2016). If a rotating gantry is available, the pCT can be potentially adopted for patient positioning verification (Cassetta *et al* 2019) (instead of the CBCT) and directly for treatment planning adaptation (instead of the deformed treatment planning CT or the scattered corrected CBCT) in proton therapy. However, geometrical and dosimetric constraints can prevent the rotation of the ion imaging detectors and thus a proper tomographic image reconstruction (Gianoli *et al* 2014, Gianoli *et al* 2016). Therefore, a 2D–3D DIR that adapts the treatment planning CT (‘3D’) to the pRads (‘2D’) is an attractive workflow to be explored, which could relax demands on in-room integration of proton imaging and could considerably reduce imaging dose for ART.

This study extends previous work using controlled transformations in analytical simulations of anthropomorphic phantoms (Palaniappan *et al* 2020) to clinical-like scenarios based on two patient datasets. A realistic deformation is derived from a CBCT of the same patient and applied to the treatment planning CT to investigate the compensation of inter-fractional anatomical changes with respect to the pRads. Rigid transformations between the treatment planning CT and the pRads are also applied to provide the investigation with the contribution of inaccuracies in patient positioning. Monte Carlo simulations of integration and list-mode pRads are performed based on the x-ray CT. The extension of the investigation to realistic clinical-like scenarios addresses also the development of stopping criteria, specifically intended to handle the convergence of the 2D–3D DIR in absence of the ground truth pCT, and the implementation of computational optimization (i.e. random sampling of the objective function computation), thus paving the way for envisioned computational efficiency of the 2D–3D DIR algorithm towards future clinical application. In addition, the influence of the compromise between proton statistics and number of pRads is studied to investigate the accuracy of the 2D–3D DIR under comparable imaging dose conditions. Finally, the role of the axial field of view (FOV) on the accuracy of the compensation of the rigid transformations, for different proton statistics, is assessed.

Table 1. Geometrical parameters adopted in Monte Carlo simulations of pRads.

Patient data	Geometrical parameters	
	Patient #1	Patient #2
Pixel size	0.1074 × 0.1074 cm	0.1074 × 0.1074 cm
Slice thickness	3 mm	3 mm
Image size	314 × 314 pixels	314 × 314 pixels
Number of slices	10, 20, 40	10
Rad angles	0°, 10°, 20°, 30°, 40°, 50°, 60°, 70°, 80°, 90°, 100°, 110°, 120°, 130°, 140°, 160°, 170°	0°, 20°, 40°, 60°, 80°, 90°, 100°, 120°, 140°, 160°

Materials and methods

Clinical data and Monte Carlo simulations

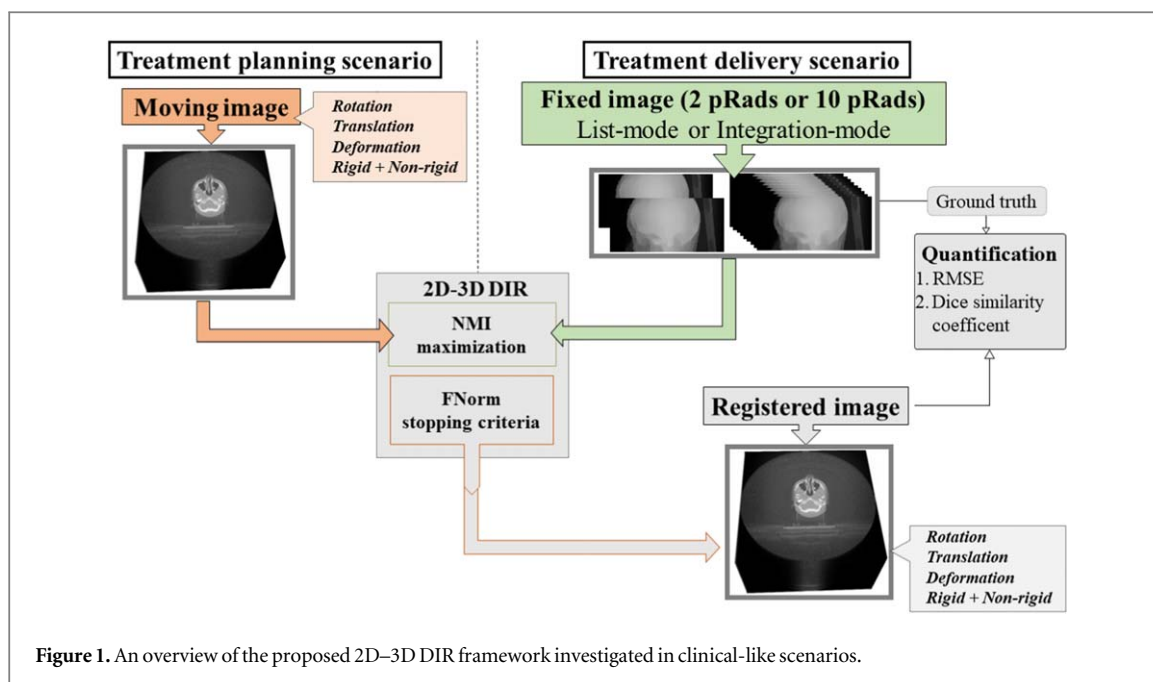
A clinical x-ray CT of a head and neck cancer patient (patient #1 in the following) and a brain tumor patient (patient #2 in the following) treated with intensity modulated photon therapy at the Department of Radiation Oncology at the Universitätsklinikum der Ludwig-Maximilians-Universität München are considered to simulate different clinical-like scenarios. The CT is converted to the ground truth pCT relying on a clinical-like monotonic calibration curve mapping the Hounsfield Units (HUs) of the CT into RSPs. The ground truth pCT is adopted in FLUKA-based Monte Carlo simulations of pRads for list-mode and integration-mode detector configurations in clinical-like pencil beam scanning, relying on a customized simulation framework (Meyer *et al* 2019). List-mode and integration-mode data are stored proton-wise and pencil beam-wise, respectively, for each Rad angle and slice. For integration-mode data, the mode WET (the WET value with maximum occurrence) is calculated from the obtained WET histogram. The nominal pencil beam energy is set equal to 199.44 MeV and a beam spot size of full width at half maximum equal to 8.5 mm is considered (Parodi *et al* 2012). For patient #1, two different proton statistics of 400 and 10000 primary protons per pencil beam are considered, thus corresponding to low and high imaging dose conditions. Small, intermediate and large FOVs are defined based on the consideration of a different number of slices. The small FOV (10 slices, 3 cm) includes the lower part of the brain and the nasal cavity. The intermediate FOV (20 slices, 6 cm) extends to the chiasm and the large FOV (40 slices, 12 cm) includes also the upper part of the brain. For the large FOV, the physical dose for each pRad is quantified as ~0.01 mGy and ~0.26 mGy, for low and high proton statistics, respectively. For patient #2, only the low imaging dose condition in combination with the small FOV is considered. Geometrical parameters adopted in Monte Carlo simulations of pRads are summarized in table 1.

Investigated clinical-like scenarios

A realistic deformation field is obtained by means of 3D–3D DIR of the clinical x-ray CT to a CBCT, acquired for patient positioning verification prior to treatment delivery. The CBCT is selected according to the largest time distance (i.e. seven and three weeks for patient #1 and patient #2, respectively) with respect to the x-ray CT. Subsequently, each component of the deformation field is multiplied roughly by a factor of 2 to amplify the anatomical changes while keeping them realistic. The deformation field is then applied to the ground truth pCT to reproduce inter-fractional anatomical changes in the treatment planning CT. The treatment planning CT, originally calibrated as the ground truth pCT, is provided with typical calibration inaccuracies by applying controlled RSP inaccuracies to the (accurate) calibration curve. The inaccuracies are randomly sampled from a uniform distribution limited within ± 0.05 (Gianoli *et al* 2020). Rigid transformations are also considered, thus eventually complementing the anatomical changes with the contribution of inaccuracies in patient positioning (i.e. couch and pillow alignment). The treatment planning CT is either translated by 6 pixels along latero-lateral and cranio-caudal directions or rotated by 5° for rigid transformations.

For list-mode data, only the 2 pRads are selected due to memory limitation (250GB), whereas for integration-mode data each of the 10 pRads are considered (table 1). Relying on integration-mode data from patient #1, the effect of large, medium and small FOVs on the accuracy of the compensation of the rigid transformations is investigated. Moreover, for small FOV, the high proton statistics is progressively reduced while increasing the number of pRads, thus investigating the compromise under comparable imaging dose conditions. Proton statistics reduction is implemented as a random selection of the proton trajectories for each pencil beam and the increasing pRads are selected while maximizing the angular separation. The imaging dose is therefore maintained approximately constant.

An overview of the 2D–3D DIR framework considering investigated clinical-like scenarios is shown in figure 1. Relying on the results of our previous work (Palaniappan *et al* 2020), the normalized mutual information is adopted as a metric in radiographic domain, where fixed image are the pRads and the moving image is the



treatment planning CT, calibrated according to both accurate or inaccurate calibration curves. Within each iteration of the 2D–3D DIR, the treatment planning CT is compensated by the optimized deformation field and the corresponding radiographies are calculated according to the specific forward-projection model of the detector configuration (Palaniappan *et al* 2020). The Frobenius norm (or Euclidean norm) of the Jacobian of the deformation field (FNorm) is proposed as a metric to define a stopping criterion of the iterative optimization (Peroni *et al* 2016). As the Jacobian of the deformation field is the matrix of the first-order partial derivative of the deformations (Vercauteren *et al* 2013), it carries information about the local smoothness of the deformation field. Therefore, its norm correlates with the global smoothness of the deformation field. The 2D–3D DIR foresees 15 iterations in 3 stages at 64, 32 and 16 as grid spacing, completed only for integration-mode data. In each stage, the global parameters of the rigid transformation are taken over by the local parameters of the non-rigid transformation, which represents a challenge for the developed algorithm. The stages for list-mode data are limited to two, due to computational time (few days for high proton statistics). Relying on the integration-mode data from patient #1, a random sampling of the objective function computation is implemented and investigated to optimize the computational performance of the optimization algorithm (Klein *et al* 2007).

Performance quantification

The performance of the 2D–3D DIR is evaluated in comparison to the conventional 3D–3D DIR of the accurately or inaccurately calibrated treatment planning CT with the ground truth pCT, provided with the same registration parameters as the 2D–3D DIR. Relying on the ground truth pCT (excluding air, treatment couch and patient pillow), the RMSE (intensity-based in image domain) and the dice similarity coefficient (volume-based) are adopted as metrics for accuracy quantification. Relying on clinical segmentation of regions of interest (including organs at risk) on the ground truth pCT, the left and right eyes, brain and brain stem are chosen for the volume-based quantification for patient #1. To do that, the regions of interest are deformed according to the obtained rigid and non-rigid transformations.

Results

Rigid transformations

The intensity-based quantification in function of the iterations when compensating the rotation and translation from integration-mode data using 2 pRads and 10 pRads is shown in figure 2 for patient #1 (in figure A1 for patient #2). The compensation of the applied transformations from list-mode data using 2 pRads are shown in figure 3 for patient #1 (in figure A2 for patient #2). The volume-based quantification in function of the stages when compensating the rotation and translation from both list-mode and integration-mode data is reported in appendix (figures A5 and A6). The small difference between the two proton statistics, appreciable with 2 pRads, vanishes with 10 pRads. This difference is not necessarily in favor of the high proton statistics (figure 2(c)). The impact of the inaccurate calibration of the treatment planning CT results negligible.

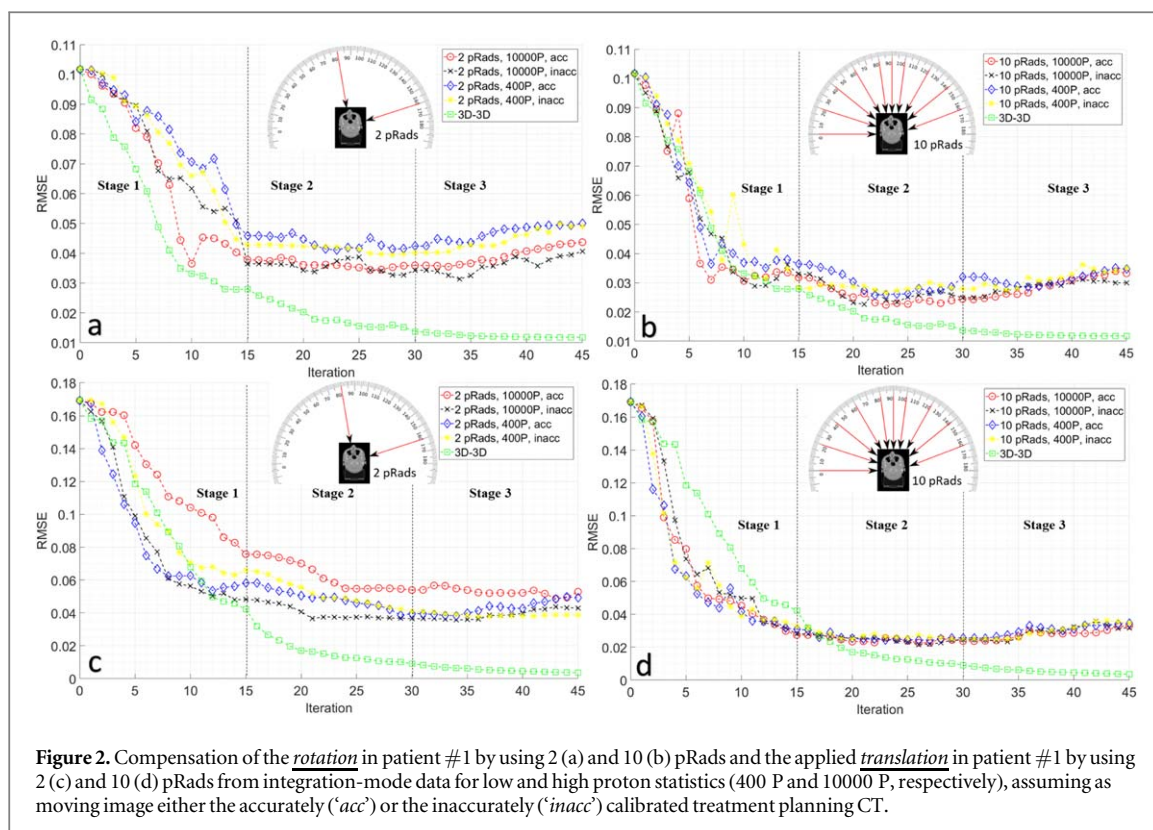


Figure 2. Compensation of the rotation in patient #1 by using 2 (a) and 10 (b) pRads and the applied translation in patient #1 by using 2 (c) and 10 (d) pRads from integration-mode data for low and high proton statistics (400 P and 10000 P, respectively), assuming as moving image either the accurately ('acc') or the inaccurately ('inacc') calibrated treatment planning CT.

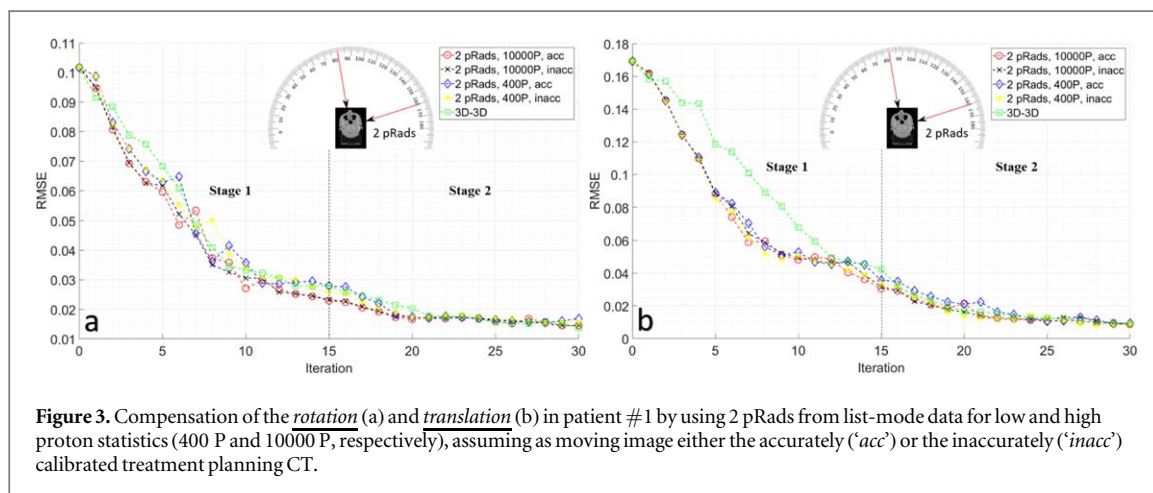
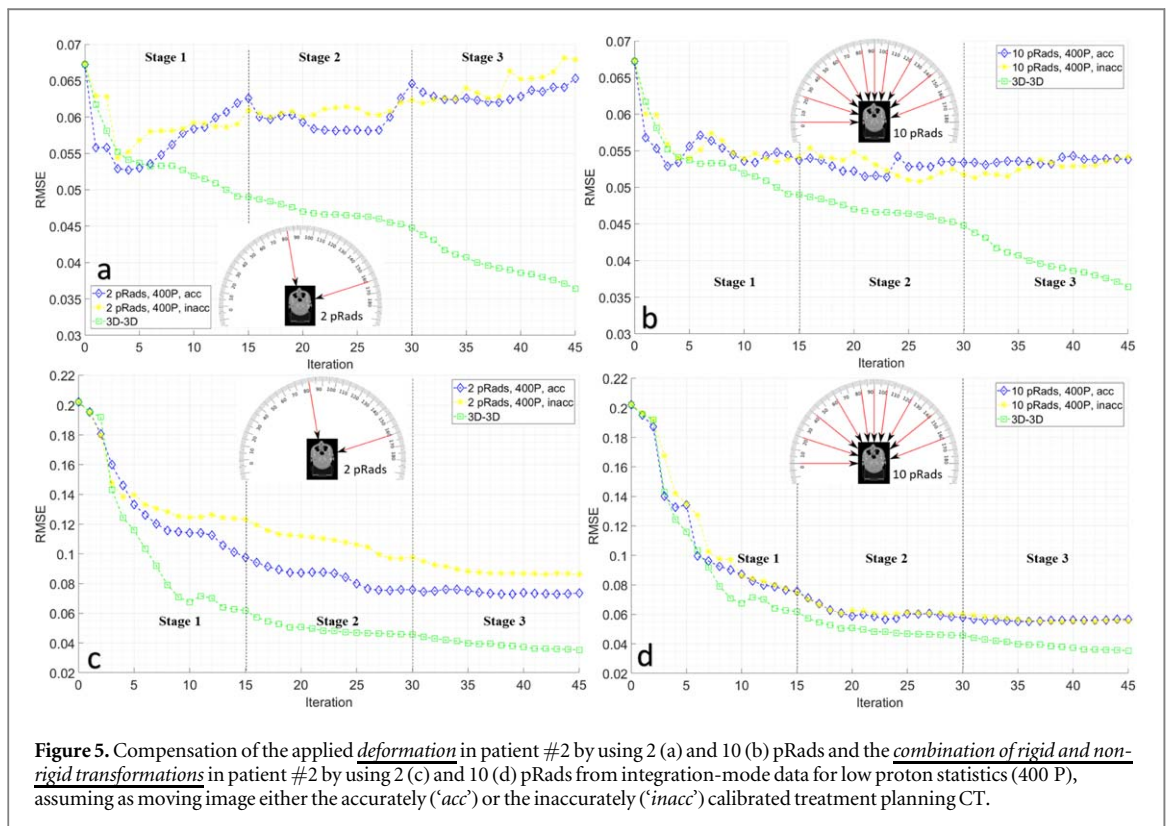
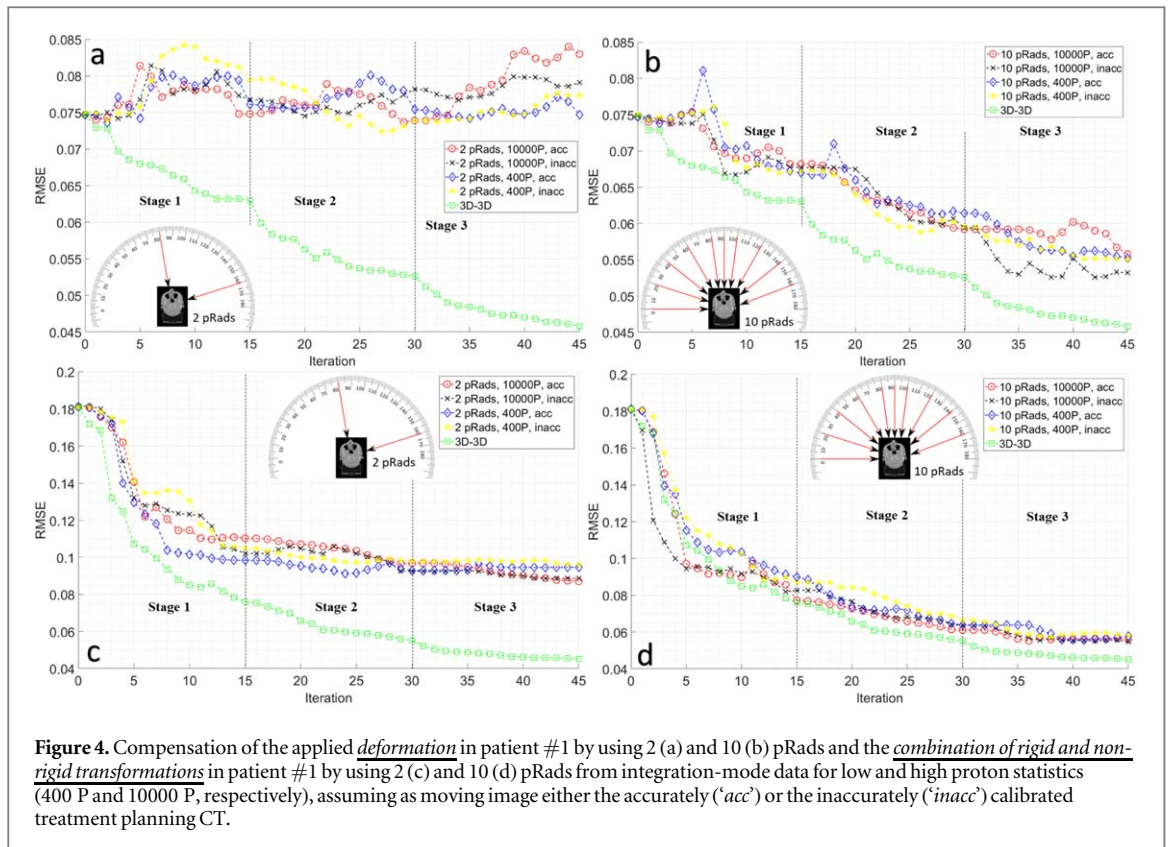


Figure 3. Compensation of the rotation (a) and translation (b) in patient #1 by using 2 pRads from list-mode data for low and high proton statistics (400 P and 10000 P, respectively), assuming as moving image either the accurately ('acc') or the inaccurately ('inacc') calibrated treatment planning CT.

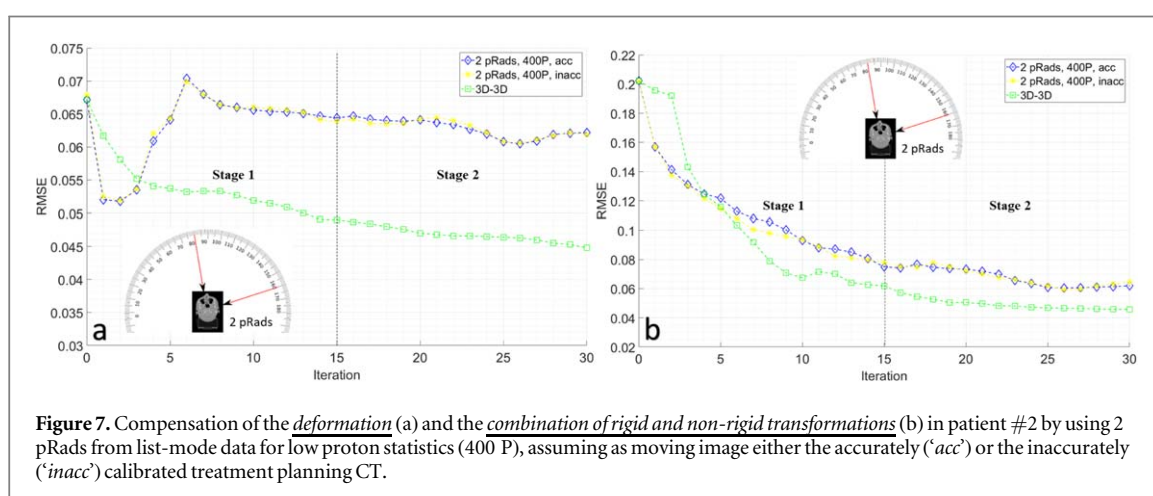
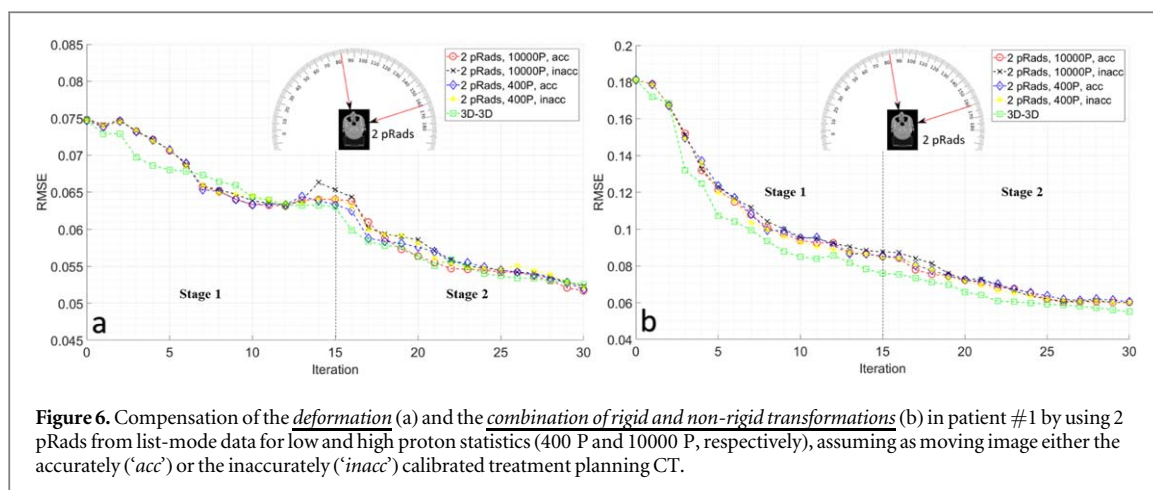
Non-rigid transformations

The compensation of the applied deformation and the combination of rigid (translation and rotation) and non-rigid (deformation) transformations for integration-mode data from patient #1 and patient #2 is reported in figures 4 and 5 respectively. The corresponding compensation from list-mode data is shown in figures 6 and 7, respectively. List-mode data achieve the accuracy of the conventional 3D–3D DIR for patient #1 and remains inferior to the conventional 3D–3D DIR for patient #2. Conversely, integration-mode data when compensating the deformation do not accurately converge with 2 pRads but tend to approach the accuracy of the conventional 3D–3D DIR with 10 pRads, although remaining less stable and less accurate. The impact of the proton statistics and the inaccurate calibration of the treatment planning CT results negligible in a similar way to the compensation of rigid transformations. The volume-based quantification in function of the stages for the compensation of the applied deformation is reported in appendix (figure A7 for integration-mode data and list-mode data). The overlay of ground truth pCT and calibrated treatment planning CT prior to and after 2D–3D DIR when compensating the combination of rigid and non-rigid transformations for both patients is shown in figure 8.



Stopping criteria

The FNORM when compensating both rigid and non-rigid transformations is reported in figures 9(c) and (d) for 10 pRads and 2 pRads from integration-mode data, respectively, and in figure 10(b) for 2 pRads from list-mode data for patient #1. The corresponding RMSE calculated with respect to the ground truth pCT is shown in figures 9(a) and (b) for integration-mode data and in figure 10(a) for list-mode data for patient #1. The FNORM



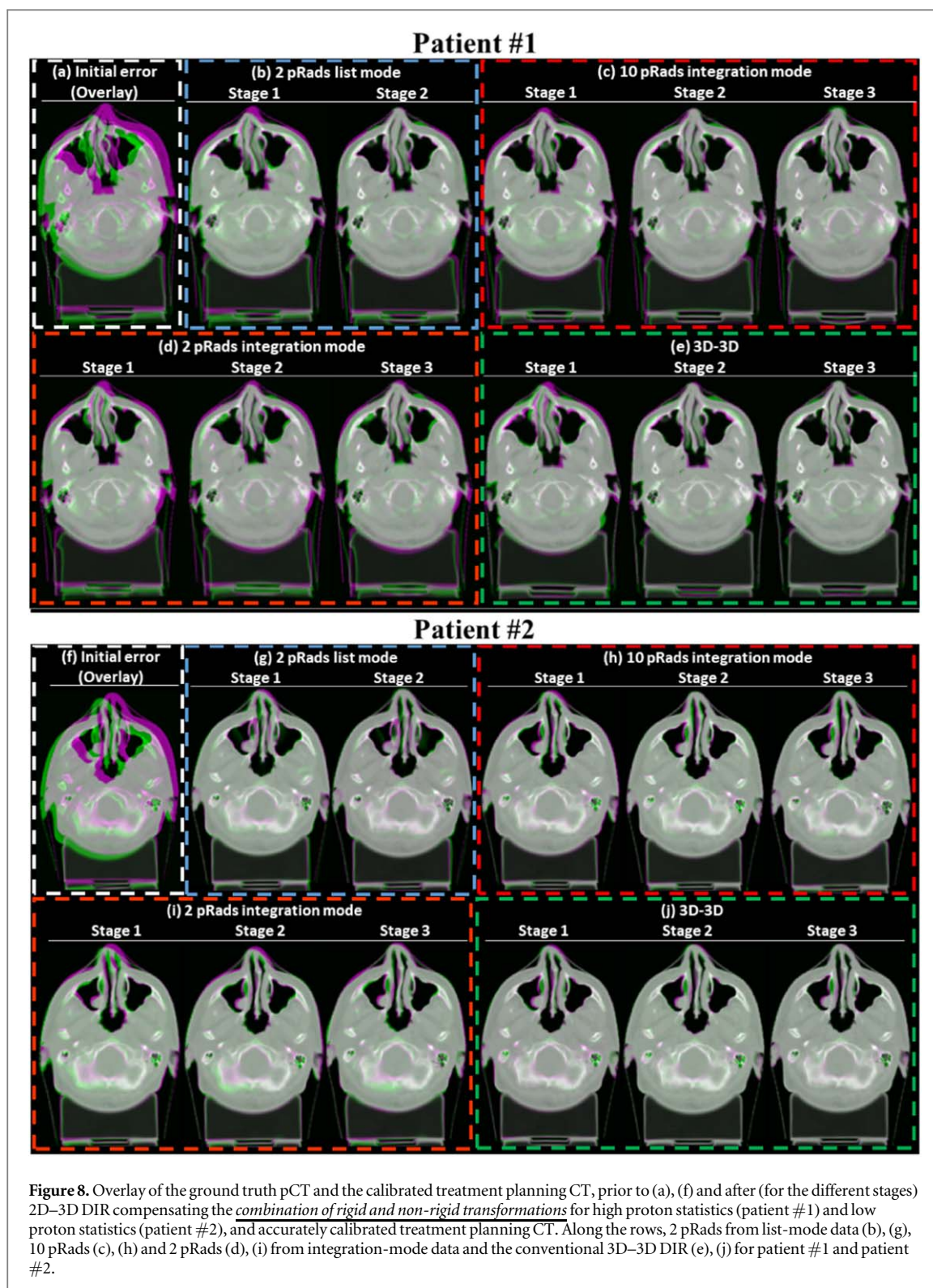
starts to increase after the RMSE reaches a plateau (rigid transformations) or a minimum (non-rigid transformations). Similar trend is noticed for patient #2 in figures A3 and A4 for integration-mode and list-mode data, respectively.

Investigated clinically orientated parameters

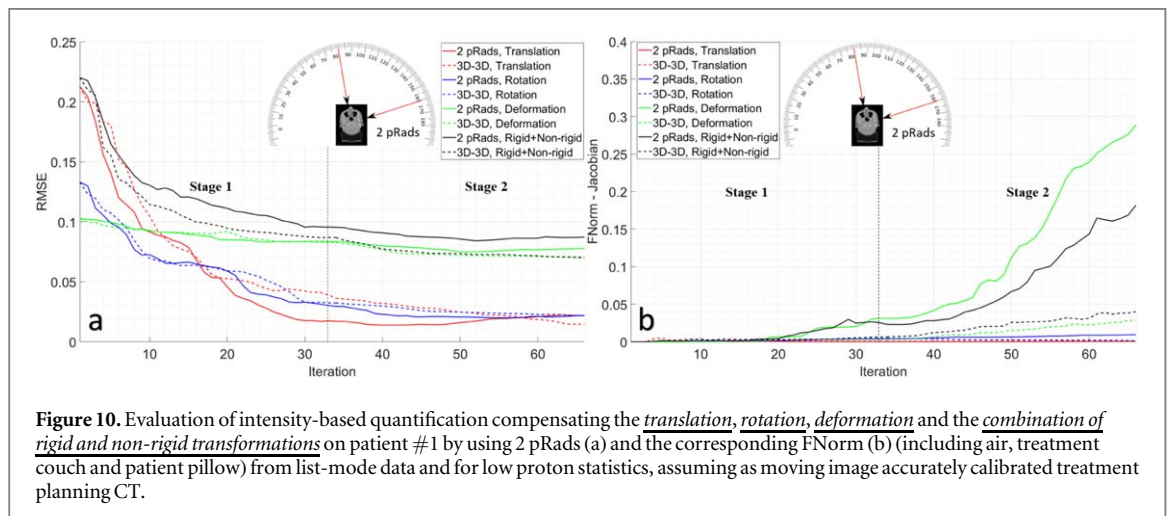
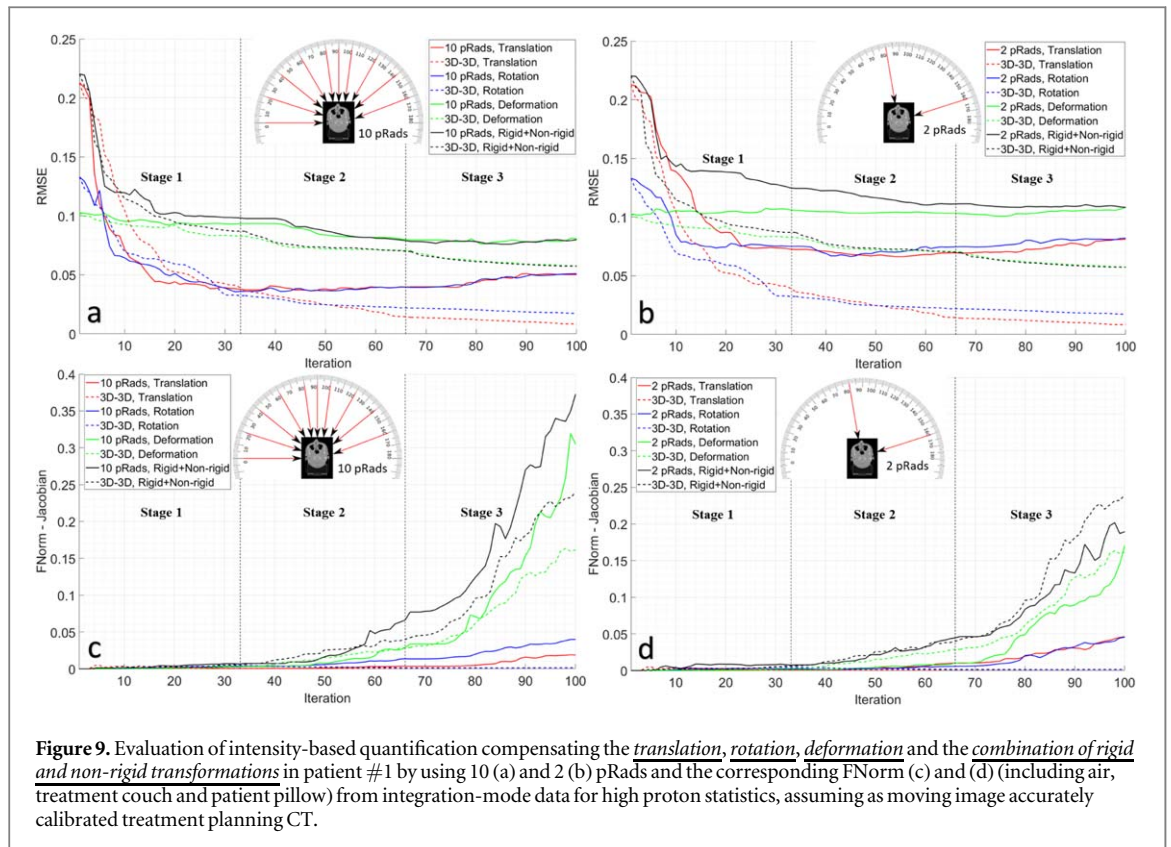
The intensity-based quantification as a function of the iterations when compensating the translation for large, intermediate and small FOVs is reported in figure 11. At low proton statistics, no remarkable differences are observed within different FOVs and between the accurate and inaccurate calibrated treatment planning CT. At high proton statistics, the larger FOV seems to benefit the accuracy; however, the smaller FOV in combination with the inaccurate calibrated treatment planning CT performs similar to the large FOV. Results for different random sampling of the objective function computation in the iterative optimization of the 2D–3D DIR are summarized in figure 12(a). A random sampling equal to 30% guarantees the accuracy of the full sampling with a 13.5% computation time reduction of the objective function. The impact of proton statistics with respect to progressively increasing number of pRads is reported in figure 12(b). By keeping the imaging dose constant (corresponding to the high proton statistics), the maximization of the Rad angles demonstrates to improve the accuracy of the 2D–3D DIR.

Discussions

The results of this work confirm and complement previous findings of Palaniappan *et al* (2020) in realistic clinical-like scenario. As expected, the list-mode outperforms the integration-mode in terms of achievable accuracy when compensating both rigid and non-rigid transformations in different patient datasets. The obtained accuracy when compensating the combination of rigid and non-rigid transformations for patient #1 using 2 pRads from list-mode data (RMSE equal to 0.0605) and 10 pRads from integration-mode data (RMSE equal to 0.0638) is comparable to conventional 3D–3D DIR (RMSE equal to 0.0551). However, the accuracy of



2 pRads from integration-mode data (RMSE equal to 0.0929) is slightly inferior. The attained accuracy using 2 pRads from list-mode data while compensating standalone rigid or non-rigid transformations is comparable to conventional 3D–3D DIR. For patient #1, the anatomical changes derived from the CBCT shows a large setup error to be compensated, besides anatomical (figure 8), so that the 2 pRads for list-mode data capture their major components (figure 6(a)). For patient #2 instead, the list-mode remains superior compared to integration-mode but not able to keep up with the 3D–3D DIR, especially when compensating the deformation (figure 7(a)). The anatomical changes derived from the CBCT of this patient data are widespread within the brain and nasal cavity (figure 8). Therefore, the 2 pRads for list-mode data does not fully compensate for the anatomical changes.



Proton statistics do not play a crucial role for list-mode data as well as for integration-mode data. The stability of the results is affected by the limited amount of information provided by integration-mode data, especially for 2 pRads. In compensating rigid transformation, the redundant information provided by larger FOVs is expected to provide better accuracy. Different from local deformations, the rigid displacement involves the entire patient/couch. However, the influence of redundant information is observed only for high proton statistics, with exception when combining the small FOV with the inaccurately calibrated treatment planning CT. The typical calibration inaccuracies do not negatively affect the 2D–3D DIR for both patients. Similar to what observed in previous work (Palaniappan *et al* 2020), the reduced accuracy of the information enables the searching space of the 2D–3D DIR to broaden. In this work, this effect penalizes the benefit of a higher proton statistics over a lower proton statistics when only 2 pRads are provided, makes irrelevant larger FOVs over smaller FOVs in low proton statistics and plays a positive role with smaller FOV in presence of additional inaccuracies in high proton statistics. The Monte Carlo simulation of pRads was in a clinically acceptable imaging dose level. The imaging dose of 180 pRads is much lower than the commercial x-ray tomography (Meyer *et al* 2019).

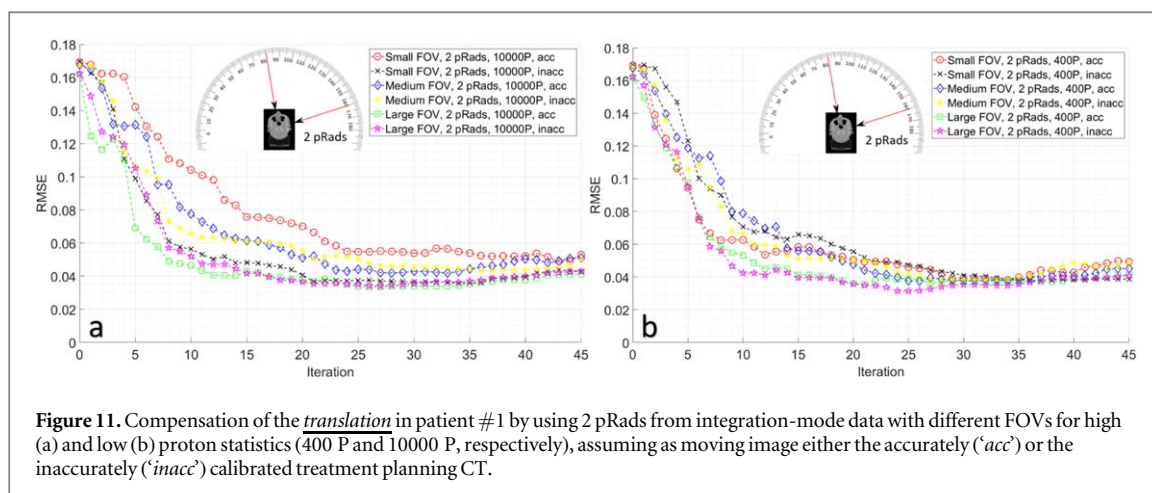


Figure 11. Compensation of the *translation* in patient #1 by using 2 pRads from integration-mode data with different FOVs for high (a) and low (b) proton statistics (400 P and 10000 P, respectively), assuming as moving image either the accurately ('acc') or the inaccurately ('inacc') calibrated treatment planning CT.

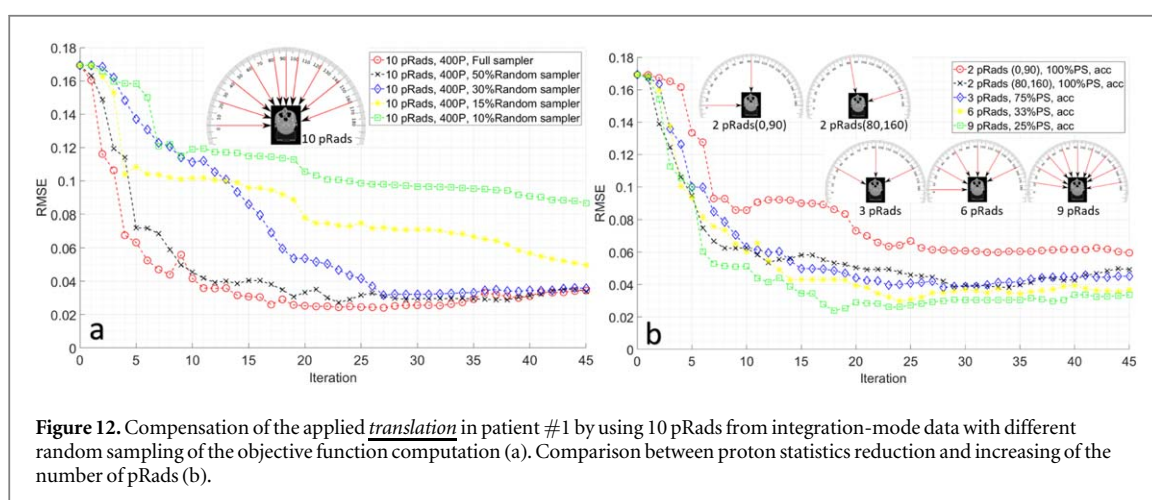


Figure 12. Compensation of the applied *translation* in patient #1 by using 10 pRads from integration-mode data with different random sampling of the objective function computation (a). Comparison between proton statistics reduction and increasing of the number of pRads (b).

The superiority of list-mode data is computationally limited to perform in finer grid spacing thus unable to foresee the maximum achievable accuracy. Around 30% random sampling of the objective function computation is sufficient to achieve the same accuracy as for 2D–3D DIR with full sampling (100%). Further reductions (15% or 10% random sampling) require additional iterations to achieve comparable results of the full sampling with a reduction in computation time of $\sim 28\%$ or $\sim 48\%$. The latter improvement contributes as $\sim 11\%$ of the overall 2D–3D DIR computation time, which includes the transformation of the compensated image (i.e. B-spline parameterization) and the analytical calculation of the corresponding radiographies (i.e. forward-projection). Therefore, in combination with the random sampling of the objective function computation, specific optimization of the computational efficiency relevant to the constitutional elements of the 2D–3D DIR framework is required. Specifically, the rigid transformation could be retained to the first stage of the registration, thus being disentangled by the non-rigid transformation in the subsequent stages. This is expected to provide an alternative to the combination of both rigid and non-rigid transformations within each stage of the deformable image registration algorithm, aiming at faster convergence.

In DIR, the stopping criteria are mainly determined by setting a maximum number of iterations as a parameter of the optimization algorithm. When the stability of the convergence of the 2D–3D DIR degrades with iterations due to limited amount and accuracy of the information provided by the pRads, stopping criteria alternative to a maximum number of iterations are necessary. The FNorm demonstrates to be indicative of the convergence of the optimization algorithm and the FNorm in function of iterations remains approximately constant until a break-up point (i.e. when it starts increasing). This break-up point could be unequivocally identified as an abrupt change in the first derivative of the FNorm trend, correlating with an unwanted deterioration of the smoothness of the deformation field. When compensating rigid transformations from list-mode data, the FNorm does not increase, as the optimization algorithm robustly converge to the applied deformation field without deteriorating in function of iterations. Therefore, the eventual deterioration, identifiable by the FNorm trend, depends on the amount and the accuracy of the information provided by the pRads. Moreover, the FNorm is put forward to solve the ambiguity in previous findings (Palaniappan *et al* 2020) of the disagreements between the RMSE and the dice similarity coefficient with respect to the ground truth pCT.

When the 2D–3D DIR is far from convergence (especially in the second stage), the RMSE can improve while the dice similarity coefficient can decrease. In these cases, the RMSE demonstrates better correlation with FNorm than the dice similarity coefficient.

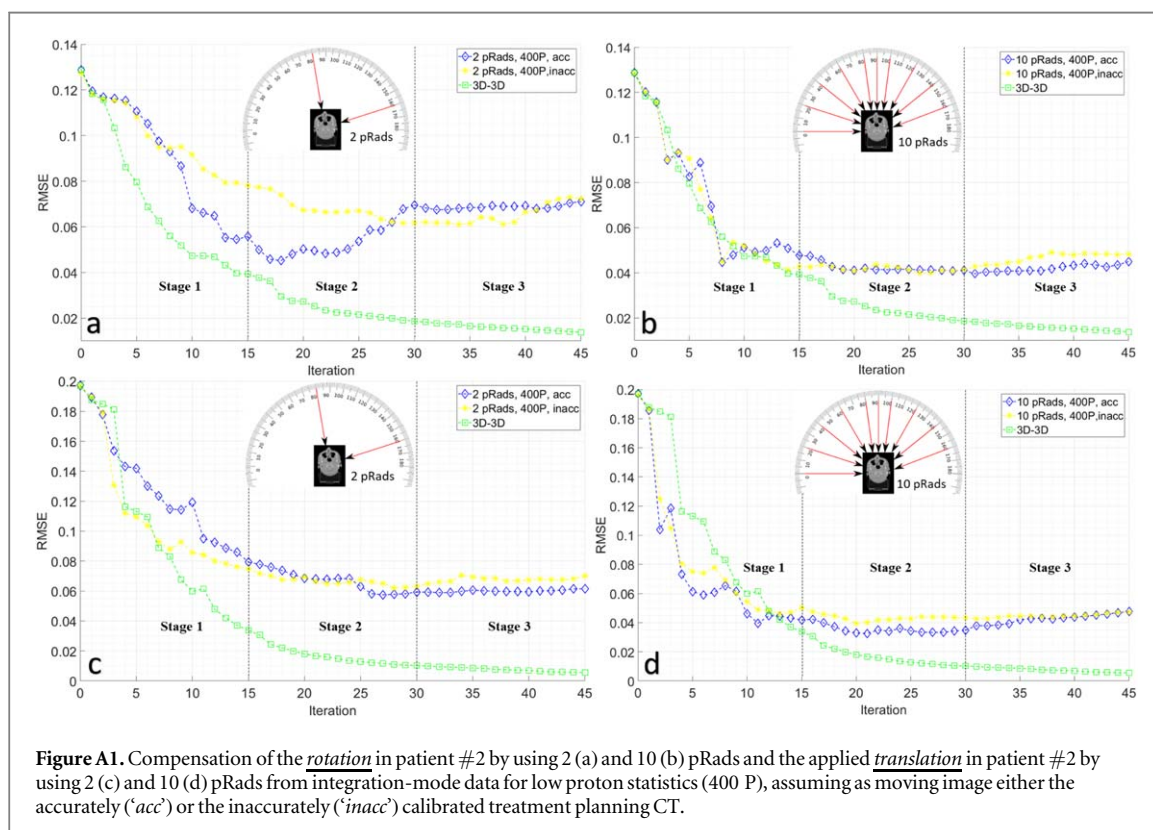
Conclusion

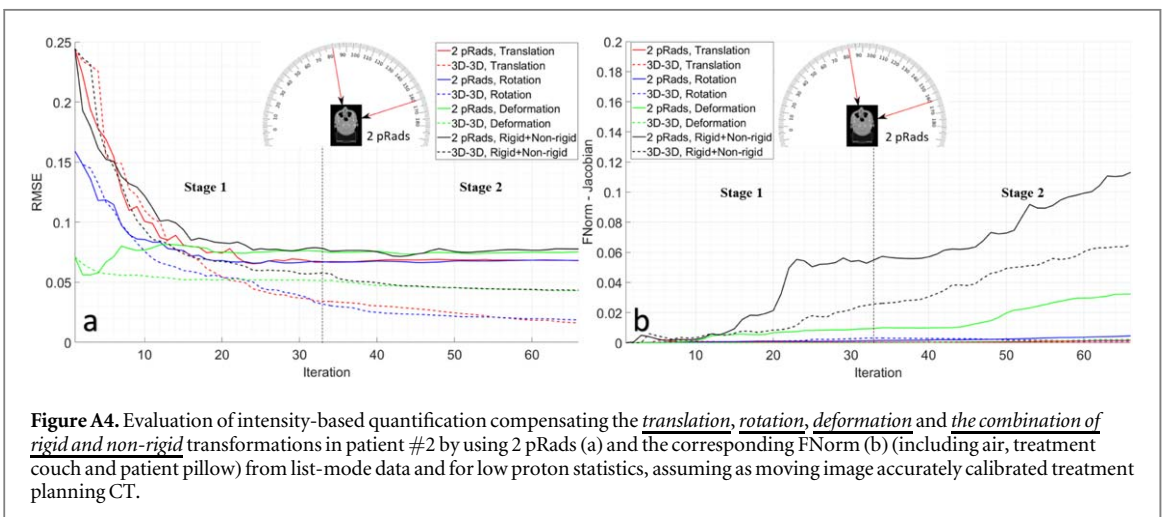
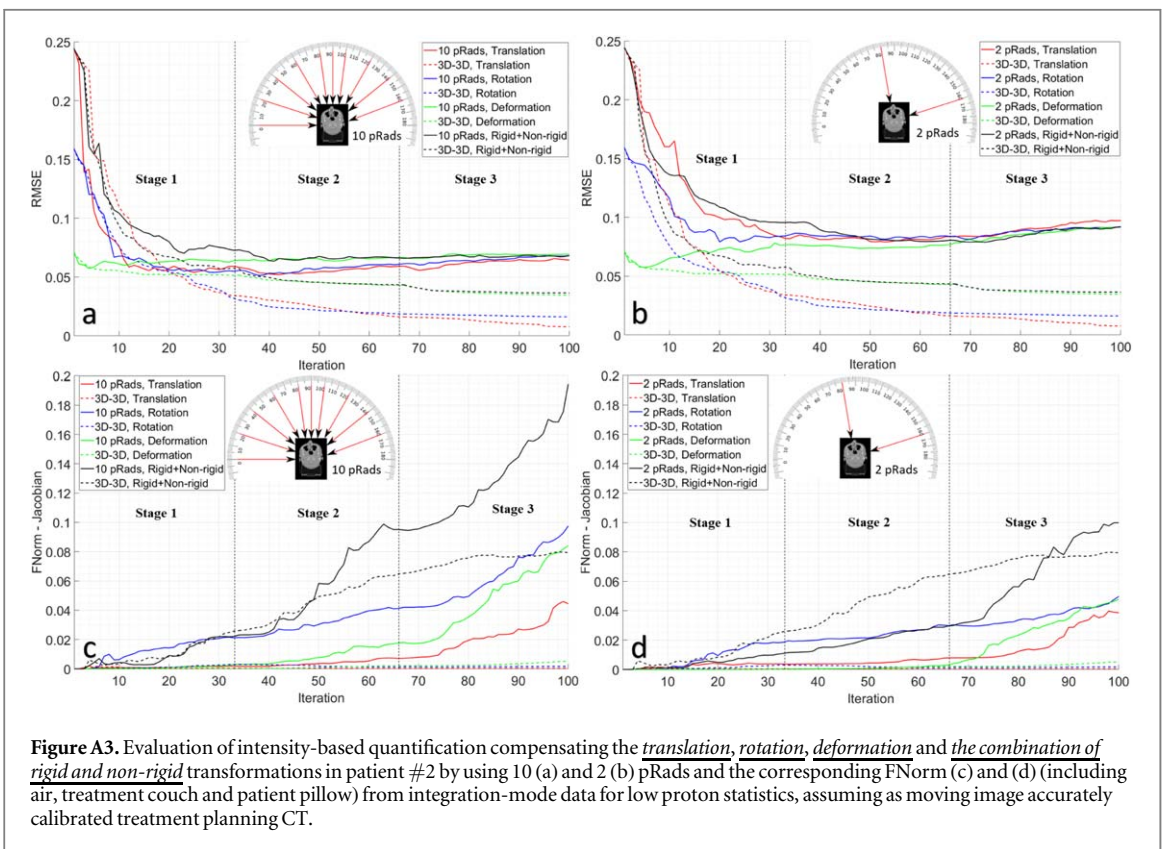
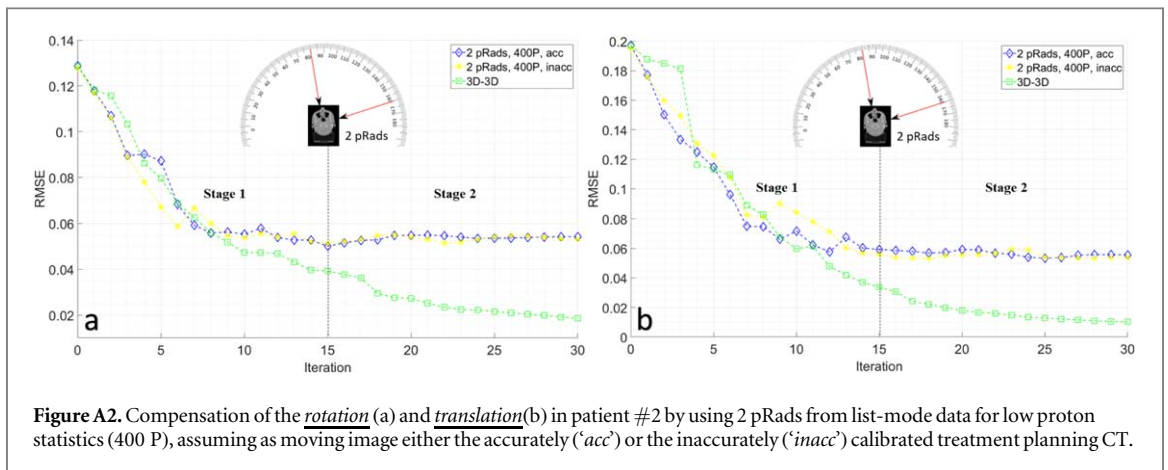
In this work, a 2D–3D DIR for adapting the treatment planning CT to applied realistic anatomical changes complemented by rigid transformations is investigated for a clinical head and neck tumor and a brain tumor in two patient datasets. A limited number of low dose proton radiographies are considered as in-room imaging. The work demonstrates the feasibility of the 2D–3D DIR for an adaptive workflow in presence of realistic inter-fractional anatomical changes. The influence of ideal integration- and list-mode detector configurations is largely perceptible in terms of accuracy, unlike the negligible impact of proton statistics. In integration-mode, the maximization of the number of pRads plays the major role over the proton statistics. Despite the effort to minimize the clinical gap using a dedicated stopping criterion and improving the computational efficiency through random sampling of the objective function, further computational optimization of the 2D–3D DIR is required to achieve the maximum convergence for list-mode data. In future, this computationally optimized framework is expected to enable an extensive clinical validation of the 2D–3D DIR in ART.

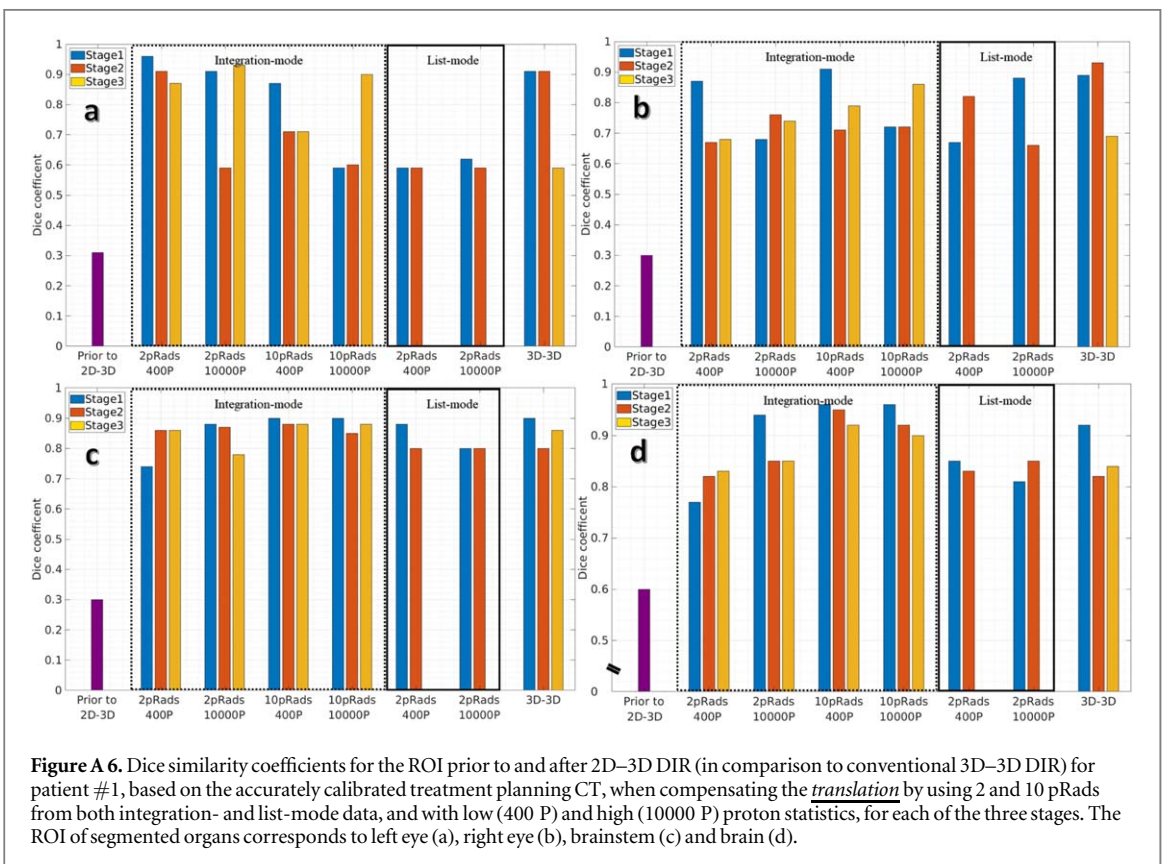
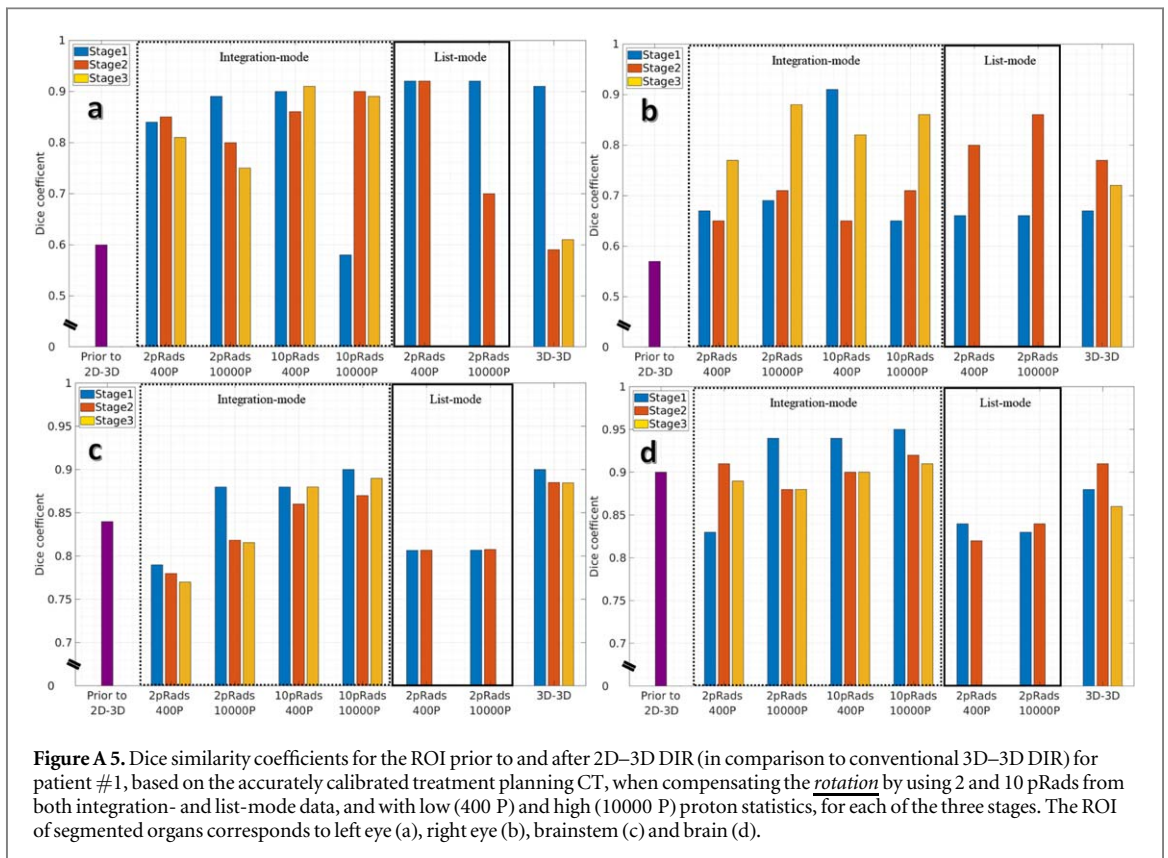
Acknowledgments

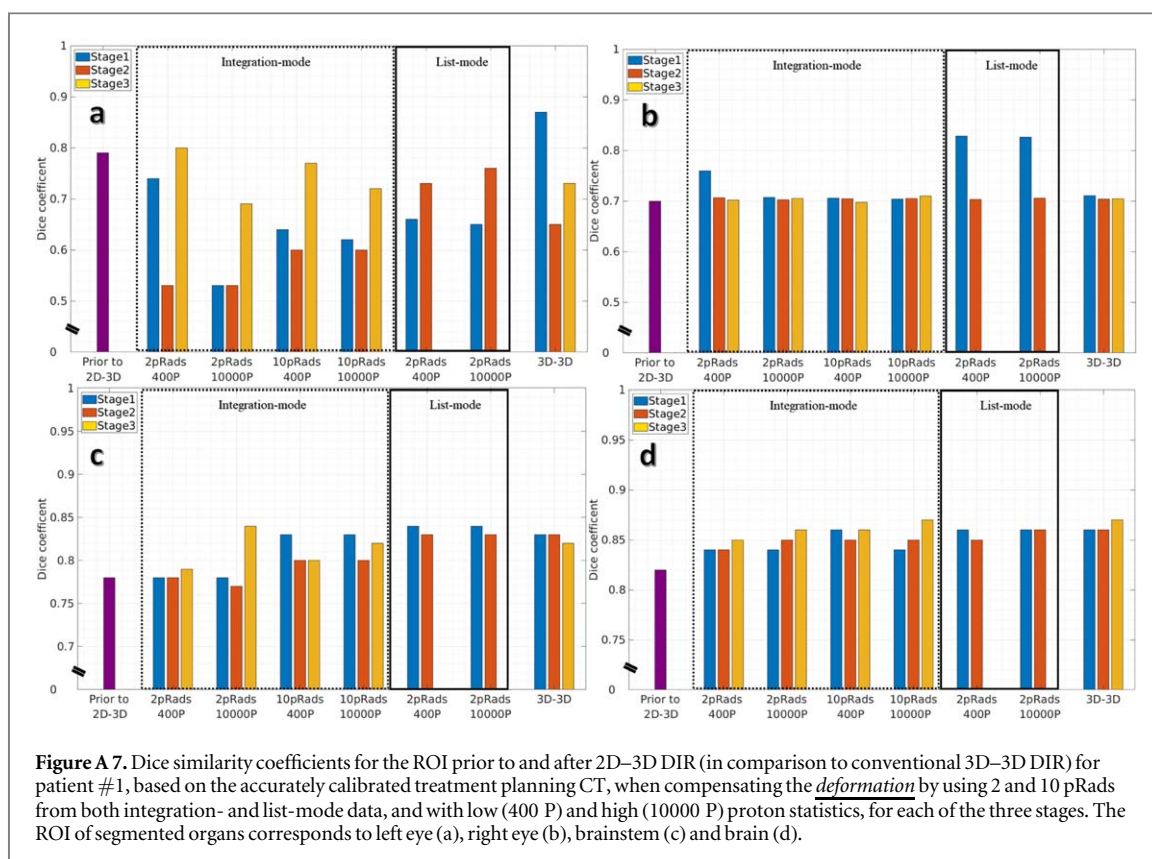
Dr Chiara Gianoli, Prof Katia Parodi, Dr Prasannakumar Palaniappan and Prof Marco Riboldi acknowledge the Deutsche Forschungsgemeinschaft (DFG) projects ‘Hybrid Imaging framework in Hadrontherapy for Adaptive Radiation Therapy’, grant #372393016, and ‘Radiography driven deformable image registration in adaptive proton therapy’, grant # 455550444.

Appendix









ORCID iDs

Sebastian Meyer <https://orcid.org/0000-0002-2510-7045>

Katia Parodi <https://orcid.org/0000-0001-7779-6690>

References

- Cassetta R, Piersimoni P, Riboldi M, Giacometti V, Bashkirov V, Baroni G, Ordonez C, Coutrakon G and Schulte R 2019 Accuracy of low-dose proton CT image registration for pretreatment alignment verification in reference to planning proton CT *J. Appl. Clin. Med. Phys.* **20** 83–90
- Fattori G, Riboldi M, Pella A, Peroni M, Cerveri P, Desplanques M and Baroni G 2015 Image guided particle therapy in CNAO room: II. Implementation and clinical validation *Phys. Med.* **31** 9–15
- Gianoli C, Fattori G, Riboldi M, Rinaldi I, Dedes G, Parodi K and Baroni G 2014 Projection-based deformable registration for tomographic imaging in ion beam therapy *Nuclear Science Symp. and Medical Imaging Conf. (NSS/MIC), 2014* (IEEE) pp 1–4
- Gianoli C, Göppel M, Meyer S, Palaniappan P, Rädler M, Kamp F, Belka C, Riboldi M and Parodi K 2020 Patient-specific CT calibration based on ion radiography for different detector configurations in 1H, 4He and 12C ion pencil beam scanning *Phys. Med. Biol.* **65** 24
- Gianoli C, Meyer S, Magallanes L, Dedes G, Landry G, Nijhuis R, Ganswindt U, Thieke C, Belka C and Parodi K 2016 Spatial resolution enhancement in integration-mode detectors for proton radiography and tomography *Radiother. Oncol.* **118** S46–7
- Johnson R P 2017 Review of medical radiography and tomography with proton beams *Rep. Prog. Phys.* **81** 016701
- Klein S, Staring M and Pluim J P W 2007 Evaluation of optimisation methods for nonrigid medical image registration using mutual information and B-splines *IEEE Trans. Image Process.* **16** 2879–90
- Kurz C, Kamp F, Park Y K, Zöllner C, Rit S, Hansen D and Hofmaier J 2016 Investigating deformable image registration and scatter correction for CBCT-based dose calculation in adaptive IMPT *Med. Phys.* **43** 5635–46
- Landry G and Hua C H 2018 Current state and future applications of radiological image guidance for particle therapy *Med. Phys.* **45** e1086–95
- Landry G, Nijhuis R, Dedes G, Handrack J, Thieke C, Janssens G and Paganelli C 2015 Investigating CT to CBCT image registration for head and neck proton therapy as a tool for daily dose recalculation *Med. Phys.* **42** 1354–66
- Meyer S, Gianoli C, Magallanes L, Kopp B, Tessonier T, Landry G and Parodi K 2017 Comparative Monte Carlo study on the performance of integration- and list-mode detector configurations for carbon ion computed tomography *Phys. Med. Biol.* **62** 3
- Meyer S, Kamp F, Tessonier T, Mairani A, Belka C, Carlson D J and Parodi K 2019 Dosimetric accuracy and radiobiological implications of ion computed tomography for proton therapy treatment planning *Phys. Med. Biol.* **64** 125008
- Meyer S, Pinto M, Parodi K and Gianoli C 2021 The impact of path estimates in iterative ion CT reconstructions for clinical-like cases *Phys. Med. Biol.* **66** 095007
- Palaniappan P, Meyer S, Kamp F, Belka C, Riboldi M, Parodi K and Gianoli C 2020 Deformable image registration of the treatment planning CT with proton radiographies for adaptive radiation therapy *Phys. Med. Biol.* **66** 4
- Park Y K, Sharp G C, Phillips J and Winey B A 2015 Proton dose calculation on scatter-corrected CBCT image: feasibility study for adaptive proton therapy *Med. Phys.* **42** 4449–59

- Parodi K 2014 Heavy ion radiography and tomography *Phys. Med.* **30** 539–43
- Parodi K, Mairani A, Brons S, Hasch B G, Sommerer F, Naumann J and Debus J 2012 Monte Carlo simulations to support start-up and treatment planning of scanned proton and carbon ion therapy at a synchrotron-based facility *Phys. Med. Biol.* **57** 12
- Peroni M, Ciardo D, Spadea M F, Riboldi M, Comi S, Alterio D and Orecchia R 2012 Automatic segmentation and online virtualCT in head-and-neck adaptive radiation therapy *Int. J. Radiat. Oncol. *Biol. *Phys.* **84** e427–33
- Peroni M, Golland P, Sharp G C and Baroni G 2016 Stopping criteria for log-domain diffeomorphic demons registration: an experimental survey for radiotherapy application *Technol. Cancer Res. Treat.* **15** 77–90
- Schneider U and Pedroni E 1995 Proton radiography as a tool for quality control in proton therapy *Med. Phys.* **22** 353–63
- Schneider U, Pemler P, Besserer J, Pedroni E, Lomax A and Kaser-Hotz B 2005 Patient specific optimization of the relation between CT-Hounsfield units and proton stopping power with proton radiography *Med. Phys.* **32** 195–9
- Schulte R W, Penfold S N, Tafas J T and Schubert K E 2008 A maximum likelihood proton path formalism for application in proton computed tomography *Med. Phys.* **35** 4849–56
- Solie J R *et al* 2020 Image quality of list-mode proton imaging without front trackers *Phys. Med. Biol.* **65** 135012
- Vercauteren T, De Gersen W, Olteanu L A, Madani I, Duprez F, Berwouts D, Speleers B and De Neve W 2013 Deformation field validation and inversion applied to adaptive radiation therapy *Phys. Med. Biol.* **58** 15